



Contents lists available at ScienceDirect

Journal of Colloid and Interface Science

journal homepage: [www.elsevier.com/locate/jcis](http://www.elsevier.com/locate/jcis)

## Hydrophobic, flexible electromagnetic interference shielding films derived from hydrolysate of waste leather scraps



Dangge Gao<sup>a,b,c,\*</sup>, Shihao Guo<sup>a,b,c</sup>, Yingying Zhou<sup>a,c</sup>, Bin Lyu<sup>a,b,c</sup>, Jianzhong Ma<sup>a,b,c,\*</sup>, Ping Zhao<sup>a,b,c</sup>, Dingjie Pan<sup>d</sup>, Shaowei Chen<sup>d,\*</sup>

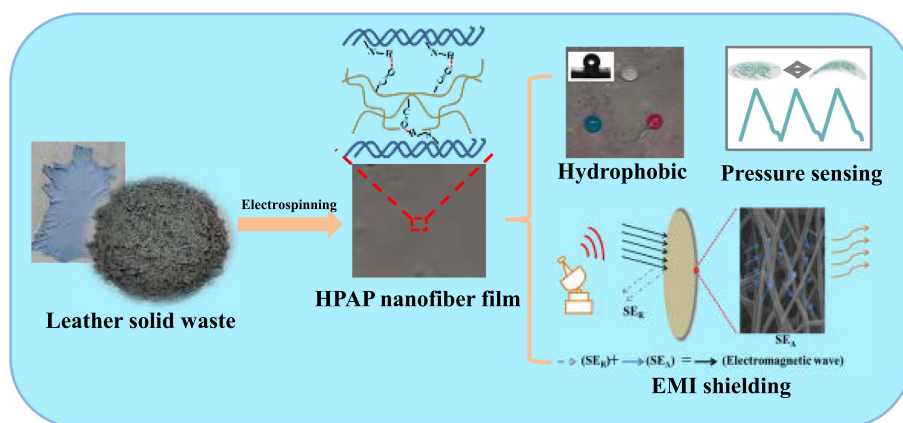
<sup>a</sup> College of Bioresources Chemical and Materials Engineering, Shaanxi University of Science and Technology, Xi'an 710021, China

<sup>b</sup> National Demonstration Center for Experimental Light Chemistry and Engineering Education (Shaanxi University of Science & Technology), Xi'an 710021, China

<sup>c</sup> Xi'an Key Laboratory of Green Chemicals and Functional Materials, Xi'an 710021, China

<sup>d</sup> Department of Chemistry and Biochemistry, University of California, 1156 High Street, Santa Cruz, CA 96064, USA

### GRAPHICAL ABSTRACT



### ARTICLE INFO

#### Article history:

Received 21 November 2021

Revised 5 January 2022

Accepted 6 January 2022

Available online 10 January 2022

#### Keywords:

Electromagnetic interference shielding

Hydrolysate of waste leather scrap

Nanofiber film

Electrospinning

Pressure sensor

### ABSTRACT

With the rapid development of wireless telecommunication technologies, it is of fundamental and technological significance to design and engineer high-performance shielding materials against electromagnetic interference (EMI). Herein, a three-step procedure is developed to produce hydrophobic, flexible nanofiber films for EMI shielding and pressure sensing based on hydrolysate of waste leather scraps (HWLS): (i) electrospinning preparation of HWLS/polyacrylonitrile (PAN) nanofiber films, (ii) adsorption of silver nanowires (AgNWs) onto HWLS/PAN nanofiber films, and (iii) coating of HWLS/PAN/AgNWs nanofiber films with polydimethylsiloxane (PDMS). Scanning electron microscopy studies show that AgNWs are interweaved with HWLS/PAN nanofibers to form a conductive network, exhibiting an electrical conductivity of  $10^5 \text{ S m}^{-1}$  and shielding efficiency of 65 dB for a 150  $\mu\text{m}$ -thick HWLS/PAN/AgNWs film. The HWLS/PAN/AgNWs/PDMS film displays an even better electromagnetic shielding efficiency of 80 dB and a water contact angle of  $132.5^\circ$ . Results from this study highlight the unique potential of leather solid wastes for the production of high-performance, environmentally friendly, and low-cost EMI shielding materials.

© 2022 Elsevier Inc. All rights reserved.

\* Corresponding authors.

E-mail addresses: [dangge2000@126.com](mailto:dangge2000@126.com) (D. Gao), [majz@sust.edu.cn](mailto:majz@sust.edu.cn) (J. Ma), [shaowei@ucsc.edu](mailto:shaowei@ucsc.edu) (S. Chen).

<https://doi.org/10.1016/j.jcis.2022.01.043>

0021-9797/© 2022 Elsevier Inc. All rights reserved.

## 1. Introduction

The development of information technology, especially the arrival of the fifth generation (5G) networks, has revolutionized the way of communication; yet the issues of electromagnetic interference (EMI) and electromagnetic pollution have been attracting increasing attention [1,2]. It is thus of both fundamental and technological significance to design and engineer high-performance EMI shielding materials [3–7]. Traditional EMI shielding materials are based on metals, such as copper, iron, cobalt, nickel, and silver, by reflecting the electromagnetic waves with almost no absorption, which can lead to secondary electromagnetic pollution [8–10]. Additionally, metal resources are increasingly scarce, and their high density, low flexibility, and poor chemical corrosion resistance all limit their practical applications [11].

Flexible and hydrophobic EMI shielding materials have become increasingly important for the long-term service of outdoor all-weather flexible wearable electrical facilities. The hydrophobic surface can not only maintain the EMI shielding effectiveness [12–14], but also endow the film with multifunctionality, such as self-cleaning, waterproof, antibacterial, and corrosion resistance. Currently, considerable efforts have been devoted to the rational design of flexible and hydrophobic EMI shielding materials by depositing conductive materials on various flexible substrates, such as nylon textiles, polymer fabrics, and carbon aerogels, followed by the coating treatment with low-surface energy materials, such as polyvinylidene fluoride (PVDF), polydimethylsiloxane (PDMS), and stearic acid (SA).

In recent years, flexible wearable pressure sensors have gained tremendous interest for unique sensing applications in, for instance, human body monitoring, electronic skin, and artificial intelligence [15–18]. They can mimic human skin by transducing external stimuli such as pressure, strain, and temperature into electrical signals. There are various sensing mechanisms for flexible wearable pressure sensors, including piezoresistance [19], piezocapacitance [20], piezoelectricity [21], and triboelectricity [22]. Among these, piezoresistive devices, which can transduce an applied pressure into a resistance signal, have been widely investigated because of their low energy consumption, cost-efficient preparation, and simple signal acquisition [23]. For instance, Li et al. [24] prepared an ultrathin flexible piezoresistive sensor with high sensitivity and a wide detection range based on a hierarchical nanonetwork structure of pressure-sensitive materials and nanonetwork electrodes, composed of Ag nanowires (AgNWs), graphene, and polyamide nanofibers.

With the increasing electromagnetic radiation in our current daily life and future aerospace technologies, the development of wearable electronic devices (e.g., pressure sensors) with EMI shielding characteristics is highly desired to mitigate potential biological damages. For instance, Chen et al. [25] prepared a porous wheat flour/carbon nanotube (CNT) composite foam by the freeze-drying process, which showed excellent pressure sensing and electromagnetic shielding properties.

Highly crosslinked conductive nanofiber films (HCC-NFs) represent another viable option, thanks to their low mass density, high conductance, and mechanical flexibility [26–30]. HCC-NFs are usually produced by attaching conductive materials to nanofiber films prepared by electrospinning [31–34]. However, the lack of intimate linkage at the crossing points in these electrospun nanofibers causes a weak connection between adjacent nanofibers [35–39]. A range of methods have been implemented to improve the interconnection. Typical physical methods include the hot-pressing method [17] and the thermal-rolling method [40], where the fibers are tightly connected by additional mechanical and thermal treatment. Chemical methods are usually based on materials containing

rich functional groups, such as formaldehyde [18], glutaraldehyde [19], and glycerol [41], which can react with functional groups on nanofibers to improve the cross-linking of nanofibers. For instance, Lai et al. [41] prepared hydrophilically engineered electrospun polyacrylonitrile (PAN) nanofiber films by reacting glycerol hydroxyl with PAN nanofiber cyanogen, followed by immersion into an aqueous solution of the conductive materials to obtain HCC-NFs. It has been found that the EMI shielding effect of HCC-NFs in the X-band can reach 22 dB.

Within this context, leather solid wastes represent an attractive option. As a biomass material, leathers come from a range of sources and possess excellent degradability [36]. In the leather process, only 20% (by weight) of the raw materials is converted into leather and the rest as solid wastes. Generally, it is difficult to dispose of these wastes, and incineration and landfill are the leading methods of treatment [37,38], which can lead to serious environmental concerns. Note that the collagen fiber of leather is a kind of structural protein, a natural polymer with three helices composed of many amino acids with a large number of acidic carboxyl groups and basic amino groups, which can be used as dipoles to dissipate microwave radiation [42–44] and as a structural scaffold to prepare HCC-NFs.

To enhance the EMI shielding effects, HCC-NFs can be reinforced with conductive materials. For instance, Chen et al. [45] prepared composite paper by blending AgNWs with cellulose nanofibers, which led to a high EMI shielding performance of 39.3 dB. Lee et al. [46] directly loaded AgNWs onto commercial cellulose paper by a repetitive dip-coating process for up to 50 cycles. As the number of dip-coating cycles increased, the cellulose/AgNW paper showed significantly improved electrical conductivity and EMI shielding effectiveness.

Herein, we describe the fabrication of hydrophobic, flexible nanofiber films based on leather solid wastes, PAN, AgNWs, and PDMS for EMI shielding and pressure sensing. Firstly, hydrolysate of waste leather scraps/PAN (HWLS/PAN) nanofiber films were prepared by electrospinning by taking advantage of the hydrogen bonding interaction between the –OH groups of HWLS and –CN moieties of PAN. The resulting nanofiber films were then dipped into an aqueous solution of AgNWs and subsequently coated with PDMS to form highly interconnected HWLS/PAN/AgNWs/PDMS composites, which exhibited a hydrophobic surface and remarkably effective EMI shielding and pressure sensing of human motions.

## 2. Experimental section

### 2.1. Materials

Leather solid wastes were acquired from Xingning Leather Company (Jiangsu, China) by the commercialized chrome tanning method using sheepskins as the starting materials. PAN powders (average molecular weight 150,000) were purchased from Aldrich. Silver nitrate ( $\text{AgNO}_3$ , 99.8%) was obtained from Tianjin Yingda Rare Chemical Reagents Factory. Ethylene glycol (EG), *N,N*-dimethylformamide (DMF, 99.8%), sulfuric acid ( $\text{H}_2\text{SO}_4$ , 98%), glacial acetic acid ( $\text{CH}_3\text{COOH}$ ), ferric chloride ( $\text{FeCl}_3$ ), polyvinylpyrrolidone (PVP, MW = 1,300,000  $\text{g mol}^{-1}$ ), and PDMS were purchased from Sinopharm Chemical Reagents Co., Ltd. Deionized water was used throughout the experiments.

### 2.2. Fabrication of HWLS

HWLS was prepared by a three-step procedure. In a typical experiment, 25 g of the leather solid waste was dispersed into 250 mL of water and 12 mL of sulfuric acid under magnetic stirring

for 6 h in a 30 ~ 35 °C water bath, before being filtered and stored in a refrigerator. The obtained products were then added to 350 g of water and 20 g of sulfuric acid under magnetic stirring for 6 h in a 30 ~ 35 °C water bath. The last treatment entailed adding the products to 100 g of water and 10 g of glacial acetic acid under magnetic stirring in a 70 ~ 75 °C water bath for 7 h.

### 2.3. Fabrication of HWLS/PAN nanofiber films

The HWLS/PAN (HP) nanofiber films were prepared by electrospinning of a DMF solution containing HWLS and 0.2 ~ 0.8 g of PAN at the HWLS: PAN mass ratio of 1:3, 1:2, 1:1, 2:1, and 3:1. The distance between the stainless steel needle (no. 20, o.d. 0.91 mm, and i.d. 0.58 mm) and collector was set at 20 cm. The needle was connected to the positive end of a high voltage source (15 kV). A rolling collector was designed to uniformly collect the nanofibers on an aluminum foil.

### 2.4. Fabrication of silver nanowires

AgNWs were prepared by adopting the polyol method reported previously [31]. In brief, PVP (0.2 g) was completely dissolved in EG (25 mL) at 60 °C under magnetic stirring. AgNO<sub>3</sub> (0.25 g) and a FeCl<sub>3</sub> salt solution (3.5 g, 0.6 mM in EG) were added into the PVP solution under stirring for 5 min to produce a uniform solution. AgNWs were produced by heating the mixture in an oil bath at 130 °C for 5 h. The product was collected by centrifugation at 4000 rpm for 10 min and rinsing with ethanol and water five times after flocculation three times with acetone. The obtained AgNWs were stored in deionized water at a concentration of 0.5 wt%.

### 2.5. Fabrication of HWLS/PAN/AgNWs nanofiber films

The HP nanofiber films prepared above (section 2.3) were dipped into the AgNWs solution (0.5 wt%) for 5 min, followed by drying in a vacuum oven at 60 °C for 10 min. The resulting HWLS/PAN/AgNWs nanofiber films for a different number of dipping cycles (*x*) were denoted as HPA-*x* (*x* = 2, 4, 6, 8, and 10).

### 2.6. Fabrication of HWLS/PAN/AgNWs/PDMS nanofiber films

PDMS was prepared by mixing the prepolymer with Dow Corning 184 at a mass ratio of 10:1 and coated onto the surface of the HPA nanofiber films obtained above. The resulting HWLS/PAN/AgNWs/PDMS (HPAP) nanofiber films were cured in an oven at 80 °C for 2 h. The fabrication process is shown in Fig. 1. To study the effect of thickness on the EMI shielding efficiency (SE), bi-layer HPAP films were prepared by the stacking hot-pressing method [17].

### 2.7. Characterization

Fourier-transform infrared (FTIR) spectroscopy tests were carried out on a Nicolet FTIR spectrometer. Scanning electron microscopic (SEM) measurements were conducted with a Hitachi S4800 SEM scope. X-ray diffraction (XRD) patterns were acquired with a Philips Analytical diffractometer at a scanning speed of 1°·min<sup>-1</sup> using Cu K<sub>α</sub> radiation ( $\lambda = 0.154$  nm) from a 35 kV X-ray source operated at 25 mA. The film thickness was measured using an electronic thickness gauge (Thwing-Albert ProGage 40\100, USA). In addition, the breaking strength and elongation at the break of nanofiber films were measured with a PT-1080 tensile tester. The electrical conductivity ( $\sigma$ ) was measured with a four-probe system (SDY-4, Guangzhou Four-Point-Probe Technology Co., Ltd., China). The EMI SE was examined by using a waveguide specimen holder (22.86 mm × 10.16 mm × 3 mm) with a vector

network analyzer (N5230A, Agilent, USA) within the frequency range of 8.2 to 12.4 GHz. The scattering parameters ( $S_{11}$  and  $S_{21}$ ) were recorded to calculate the coefficients of reflectance (*R*), absorbance (*A*), and transmittance (*T*) for the total shielding efficiency ( $SE_T$ ), microwave reflection ( $SE_R$ ), microwave absorption ( $SE_A$ ) and microwave multiple internal reflections ( $SE_M$ ) ( $SE_M$  can be negligible when  $SE_T$  is greater than 10 dB [47]) by the following equations [46,48]:

$$R = |S_{11}|^2 \quad (1)$$

$$T = |S_{21}|^2 \quad (2)$$

$$A = 1 - R - T \quad (3)$$

$$SE_R(\text{dB}) = -10\log(1 - R) \quad (4)$$

$$SE_A(\text{dB}) = -10\log\left(\frac{T}{1 - R}\right) \quad (5)$$

$$SE_T(\text{dB}) = SE_A + SE_R + SE_M \quad (6)$$

## 3. Results and discussion

### 3.1. Characterization of HP nanofiber films

The surface morphologies of the HP nanofiber films were first examined by SEM measurements. From Fig. 2, one can see that with the increase of the HWLS content, the color of the DMF dispersion of the HP spinning solution became intensified from light green to dark green (Fig. 2 insets), and the beading phenomenon started to appear. This was particularly apparent with the samples prepared at the high HWLS: PAN mass ratios of 2:1 and 3:1 (Fig. 2d-2e). Notably, the viscosity of the spinning solution decreased accordingly (Table S1), and it became increasingly difficult to form a Taylor cone. The droplets of the spinning solution were not affected by the electric field and directly dripped onto the aluminum foil. This is because PAN is a high molecular weight polymer, and the higher the content, the higher the viscosity of the spinning solution. Notably, nanofibers are woven closely at the HWLS: PAN ratio of 1:1 (Fig. 2c), as HWLS provided strong cross-linking, as compared to others.

The effect of HWLS content on the tensile strength of the HP films is depicted in Fig. 2f. At the low HWLS: PAN ratio of 1:3, the tensile strength is 5.98 MPa. With the increases of the HWLS content, the tensile strength increases first and then decreases, reaching a maximum at 6.97 MPa at the HWLS: PAN ratio of 1:1. The initial increase of the tensile strength can be ascribed to the large number of OH groups in HWLS that react with C≡N in PAN to form cross-linking networks. Yet the subsequent decline is due to a high HWLS content that greatly reduced the viscosity of the spinning solution (Table S1). This renders it difficult to form a nanofiber network. Thus, to obtain high tensile strength, the HWLS: PAN mass ratio of 1:1 was chosen for subsequent experiments.

The structures of the HP nanofiber films were then characterized by FTIR spectroscopic measurements. From Fig. 2g, PAN exhibited several characteristic vibrational bands, C≡N stretching vibration at 2240 cm<sup>-1</sup>, C=O vibration at 1667 cm<sup>-1</sup>, and C—H bending vibration at 1454 cm<sup>-1</sup>. HWLS showed the overlapping bands of N—H and O—H stretching (around 3404 cm<sup>-1</sup>), C=O stretching vibration (amide I, 1647 cm<sup>-1</sup>), and N—H bending vibration (amide II, 1545 cm<sup>-1</sup>). For the HP nanofiber films, the C≡N stretching vibration can be found at 2240 cm<sup>-1</sup>. As compared to HWLS and PAN alone, the broad peaks (O—H stretching) located between 3500 and 3000 cm<sup>-1</sup> shifted to a lower wavenumber with

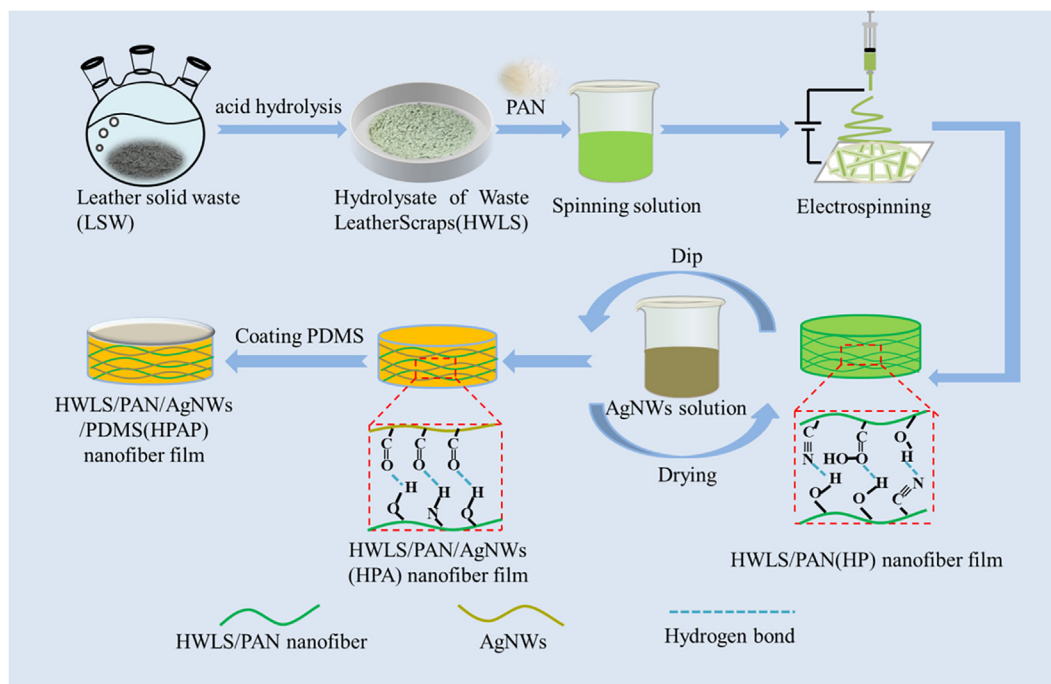


Fig. 1. Schematic diagram of the fabrication of conductive HPAP nanofiber films.

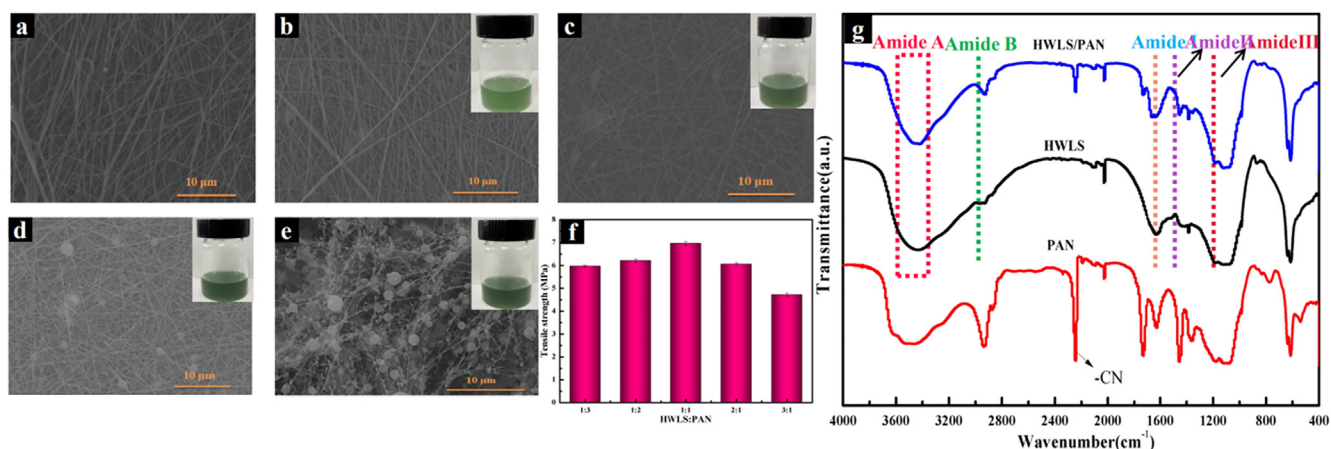


Fig. 2. SEM images of the HP nanofiber films prepared at different HWLS: PAN ratios: (a) 1:3, (b) 1:2, (c) 1:1, (d) 2:1, and (e) 3:1. (f) The corresponding tensile strength of the HP nanofiber films. (g) FTIR spectra of PAN, HWLS, and HP nanofiber films.

the HP nanofiber films, suggesting the generation of hydrogen bonds between the two components, where the hydroxyl functional groups of HWLS readily reacted with the nitrile groups in the PAN polymer chains.

### 3.2. Characterization of HPA nanofibers and EMI shielding performance

From the XRD patterns in Fig. 3a, the HP nanofiber films can be seen to possess a strong diffraction peak at  $2\theta = 17^\circ$ , corresponding to the PAN (100) crystal plane [15]. For HPA, five additional diffraction peaks can be identified at  $2\theta = 38.1^\circ$ ,  $44.3^\circ$ ,  $64.4^\circ$ ,  $77.5^\circ$ , and  $88.1^\circ$ , corresponding to the (111), (200), (220), (311), and (222) planes of face-centered cubic (fcc) Ag (JCPDS No. 4-783), respectively. This suggests the successful incorporation of AgNWs into the nanofibers.

The corresponding SEM image is shown in Fig. 3b, in which HP fibers are indicated by blue arrows, and AgNWs are indicated by red arrows. It can be seen that the HPA sample is composed of HP nanofibers, which are entangled with AgNWs in an irregular arrangement, and the elements of Ag, C, and N were distributed evenly across the sample, as manifested in elemental mapping analysis based on energy-dispersive X-ray spectroscopy (EDS, Fig. 3c–3e). Such a uniform distribution of Ag is important for the shielding of electromagnetic waves.

Notably, there is a positive correlation between the materials electrical conductivity and EMI SE [46]. Fig. 4a shows the electrical conductivity of the HPA nanofiber films prepared with different numbers of dipping cycles ( $x$ ) into the AgNWs solution. For the AgNWs-free HP nanofiber films, the electrical conductivity was estimated to be  $10^{-9} \text{ S m}^{-1}$  which increased markedly with the incorporation of AgNWs into the nanofibers. For instance, after only two dipping cycles, the electrical conductivity of HPA-2 was

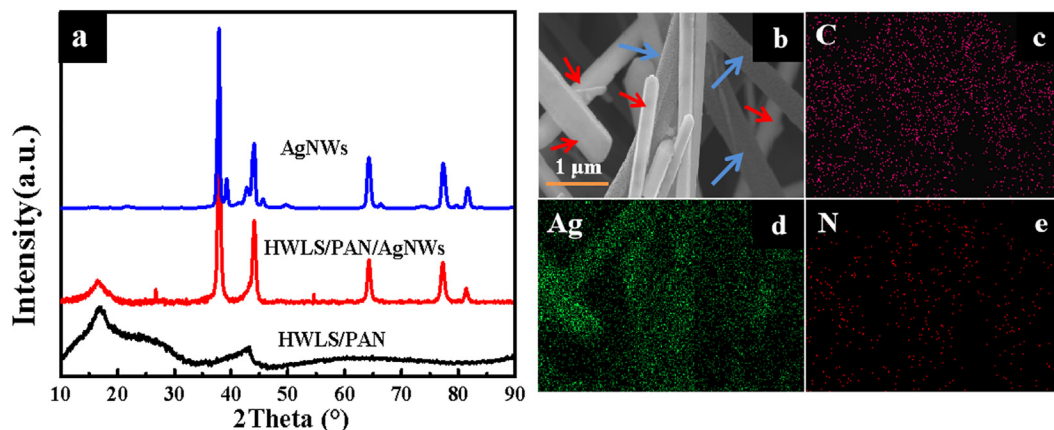


Fig. 3. (a) XRD spectra of AgNWs, HP, and HPA nanofiber films. (b) SEM image of an HPA nanofiber film, and the corresponding EDS elemental maps of (c) C, (d) Ag, and (e) N.

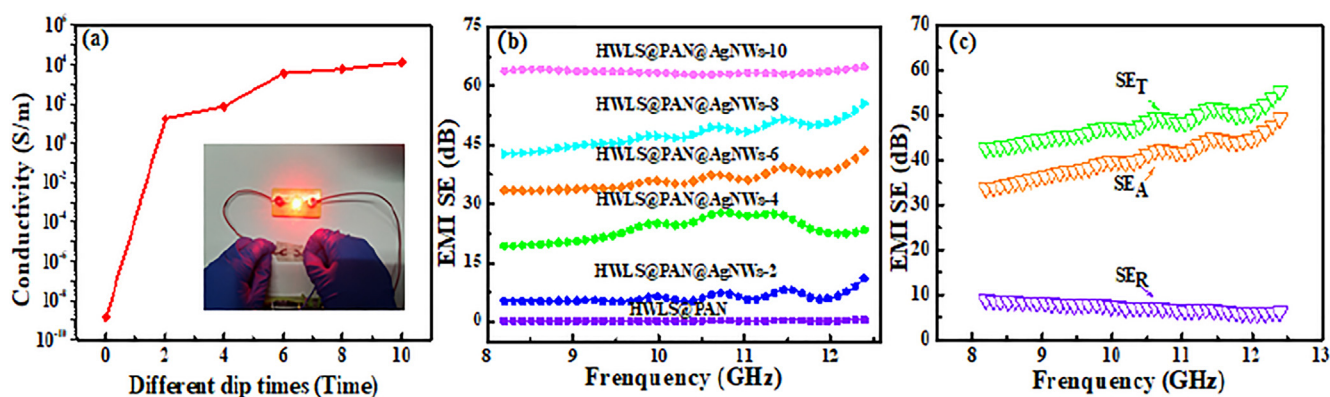


Fig. 4. (a) Electrical conductivity of HPA as a function of dip cycles into the AgNW solution. Inset is a photograph where a LED is lit up by a power source connected with HPA-6. (b) EMI performance of HPA as a function of dip cycles, and (c)  $SE_R$ ,  $SE_A$ , and  $SE_T$  of the HPA-8 sample as a function of test frequency.

almost 10 orders of magnitude higher at 12 S m<sup>-1</sup>, and after six cycles of dipping, the electrical conductivity increased further to 10<sup>4</sup> S m<sup>-1</sup>. In fact, when HPA-6 was connected with an electric wire to a power source of 3 V, a LED light board can be easily lit up (inset to Fig. 4a). This confirms the high electrical conductivity of the 3D interconnected nanofiber films.

Fig. 4b depicts the relationship between the number of dipping cycles into the AgNWs suspension and EMI SE. With 4 cycles of dipping, the EMI SE of the HPA nanofiber film was over 20 dB, most likely due to reduced porosity and enhanced electrical conductivity of the interconnected conductive structure and the 3D scaffold that effectively impeded aggregation of the conductive materials. Further dipping increased the electromagnetic shielding performance and at 10 dipping cycles, the EMI SE was 65 dB, which can completely meet the standard of commercial electromagnetic shielding materials [49].

To unravel the electromagnetic shielding mechanisms, we calculate the total shielding effectiveness ( $SE_T$ ), adoption loss ( $SE_A$ ), and reflection loss ( $SE_R$ ) from the measured S-parameter within the frequency range of 8.2 to 12.4 GHz for HPA-8. For the electromagnetic microwave,  $SE_T$  is the total sum of the contribution of  $SE_A$ ,  $SE_R$ , and multireflection loss ( $SE_M$ ),  $SE_T = SE_A + SE_R + SE_M$ .  $SE_M$  is negligible when  $SE_T$  is greater than 10 dB [20]. The results are presented in Fig. 4c, where the HPA nanofiber films can be seen to display an  $SE_T$ ,  $SE_R$ , and  $SE_A$  of -55.2 dB, -5.6 dB, and -48.5 dB (-88%  $SE_T$  at 12.4 GHz), respectively. This suggests that  $SE_A$  was a major contributor to EMI shielding efficiency, as compared to  $SE_R$  in the HPA nanofiber films.

### 3.3. EMI shielding performance of HPAP nanofiber films

The EMI shielding performance was enhanced with the HPAP nanofiber films. From Fig. 5a it can be seen that at a thickness of 150 μm, the EMI SE was estimated to be 65 dB. For highly conductive EMI shielding materials, the EMI SE is positively correlated with the electromagnetic frequency ( $f$ ), materials electrical conductivity ( $\sigma$ ) and thickness ( $t$ ), according to Simon's empirical formula,  $SE = 50 + \log(\frac{\sigma}{\rho}) + 1.7t\sqrt{\sigma f}$ . Fig. 5b shows the EMI shielding properties of a bi-layer of HPAP nanofiber films prepared by 10 dipping cycles, which featured a thickness is 320 μm, and an enhanced electromagnetic shielding efficiency of 80 dB at 10.8 GHz.

The EMI shielding process of the HPA films is illustrated in Fig. 5c. Upon the exposure of the HPA nanofiber films to external incident electromagnetic waves, a relatively small fraction of the radiation was immediately reflected back owing to impedance mismatch at the air-film interface caused by free electrons generated on the film surface. Most of the remaining waves interacted with the conductive network and became consumed by conversion into thermal energy, resulting in significant microwave absorption and energy dissipation. Meanwhile, multiple internal reflections of the electromagnetic wave could occur due to the random dispersion of AgNWs, resulting in further absorption and dissipation of the incident electromagnetic waves. In fact, almost no electromagnetic waves could pass through the film after these layers of absorption and loss.

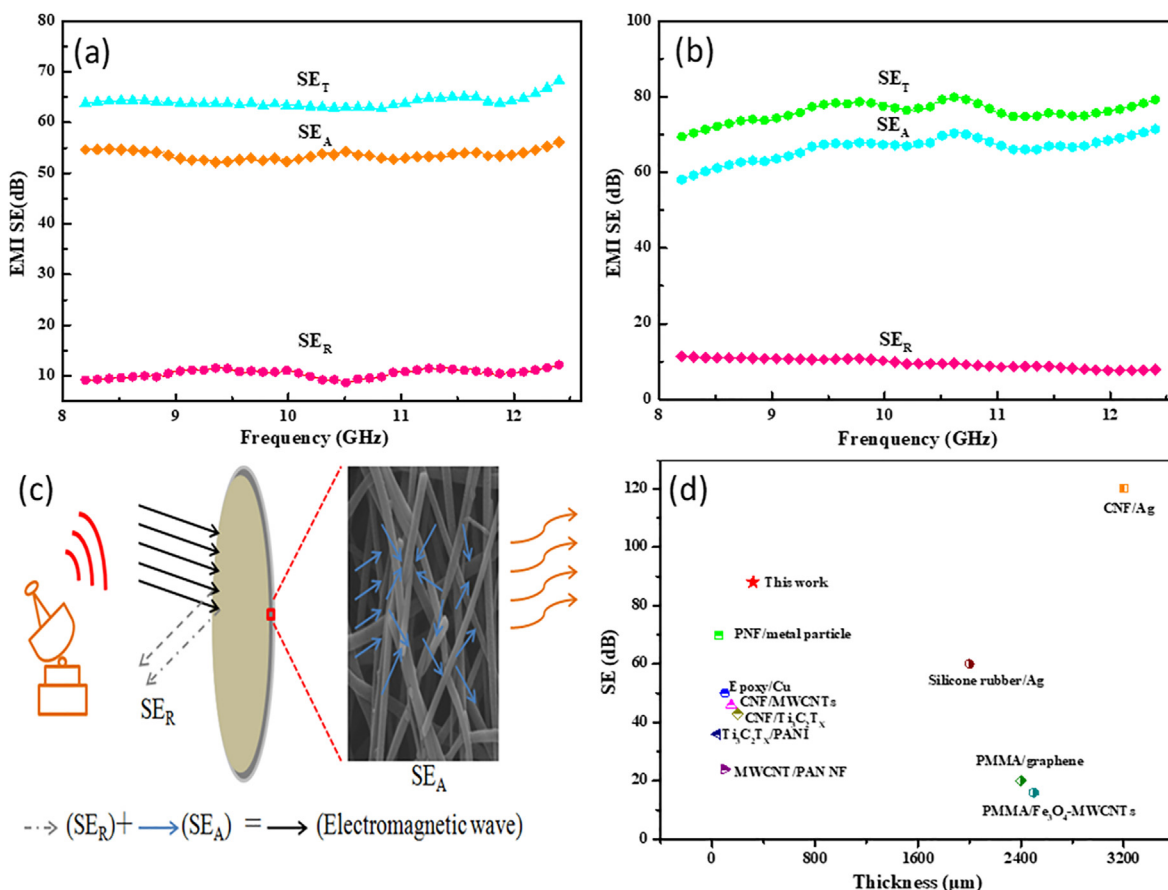


**Fig. 5.** (a)  $SE_R$ ,  $SE_A$  and  $SE_T$  of the HPAP samples as a function of test frequency. (b)  $SE_R$ ,  $SE_A$ , and  $SE_T$  of the double-layer HPAP samples as a function of test frequency. (c) Schematic illustration of the EMI shielding mechanism of the HPAP nanofiber films. (d) Comparison of EMI shielding performance vs the thickness of composite materials in published work.

Fig. 5d shows the electromagnetic shielding performance of HPAP nanofiber films. Notably, the HPAP nanofiber films exhibited a higher EMI shielding performance at a lower film thickness than leading EMI-shielding composites reported previously, such as PNF/metal particles [26],  $Ti_3C_2T_x/PANI$  [50], Epoxy/Cu [51], silicone rubber/Ag [52], PMMA/graphene [53], PMMA/ $Fe_3O_4$ -MWCNTs [54], CNF/Ag [55], CNF/ $Ti_3C_2T_x$  [41], CNF/MWCNTs [56], and MWCNT/PAN NF [57]. This suggests that the obtained HPAP nanofiber films are viable candidates for the development of new-generation multi-frequency, lightweight, and intelligent electromagnetic shielding materials.

### 3.4. Water contact angle and self-cleaning behaviors of HPAP nanofiber films

Moisture of the external environment may exert negative effects on the performance of electronic devices. Therefore, it is necessary to study the surface hydrophobic property of the EMI shielding materials. As shown in Fig. 6a, the water contact angle ( $\phi$ ) of the PAN film was estimated to be  $117.3^\circ \pm 1.12^\circ$ . Yet, for the HP nanofiber film,  $\phi$  was significantly lower at only  $15.5^\circ \pm 0.83^\circ$ , likely due to the hydrophilic groups, such as OH and COOH, in the sample. Upon the incorporation of AgNWs into the nanofibers, HPA exhibited an even lower  $\phi$  of  $4.5^\circ \pm 0.55^\circ$ . Yet, upon the coating of PDMS, the resulting HPAP nanofiber films became markedly hydrophobic at  $\phi = 132.5^\circ \pm 1.95^\circ$ .

To simulate the harsh environmental conditions, the contact angles were also measured with strong acid, base, seawater, and acid rain (Fig. 6b and 6c), where one can see that the contact angles

all remained greater than  $115^\circ$ . In fact, within the wide range of pH (1 to 14) (Figure S1), and water contact angles were all over  $105^\circ$ . This hydrophobic surface renders it possible to easily clean the materials surface. For instance, as shown in Fig. 6d, coffee powders sprayed on the HPAP surface could be quickly removed by simple water rinsing, restoring the clean film surface.

### 3.5. Sensing performance of HPAP nanofiber films

The performance of the HPAP nanofiber films as a skin piezoresistive sensor is also tested. Fig. 7a shows a schematic pressure sensing model based on HPAP nanofiber films. Without the application of a pressure onto the skin piezoresistive sensor, the layers of materials within the sensor were too far away from each other to allow effective charge transport. Yet, when a pressure was applied to the skin sensor, the electrodes were in intimate contact with the HPAP nanofiber films, resulting in the formation of electrically conductive pathways between the electrodes and the HPAP nanofiber films. Such a pressure sensor not only enables high sensitivity and a wide linear range but also offers a rapid response (ca. 250 ms), as shown in Fig. 7b. To examine the feasibility and practicability of the as-fabricated HPAP nanofiber films as a wearable sensor for human body motions, the sensor was attached to the elbow joint, and the pressure-induced resistance was monitored and depicted in Fig. 7c. Interestingly, one can see that a larger bending angle (from  $120^\circ$  to  $90^\circ$ ,  $60^\circ$ , and  $30^\circ$ ) leads to a higher current signal. Fig. 7d shows the relative current variation of the HPAP sensor under repeated tests at different working frequencies. The response signal is highly steady and independent of the load-

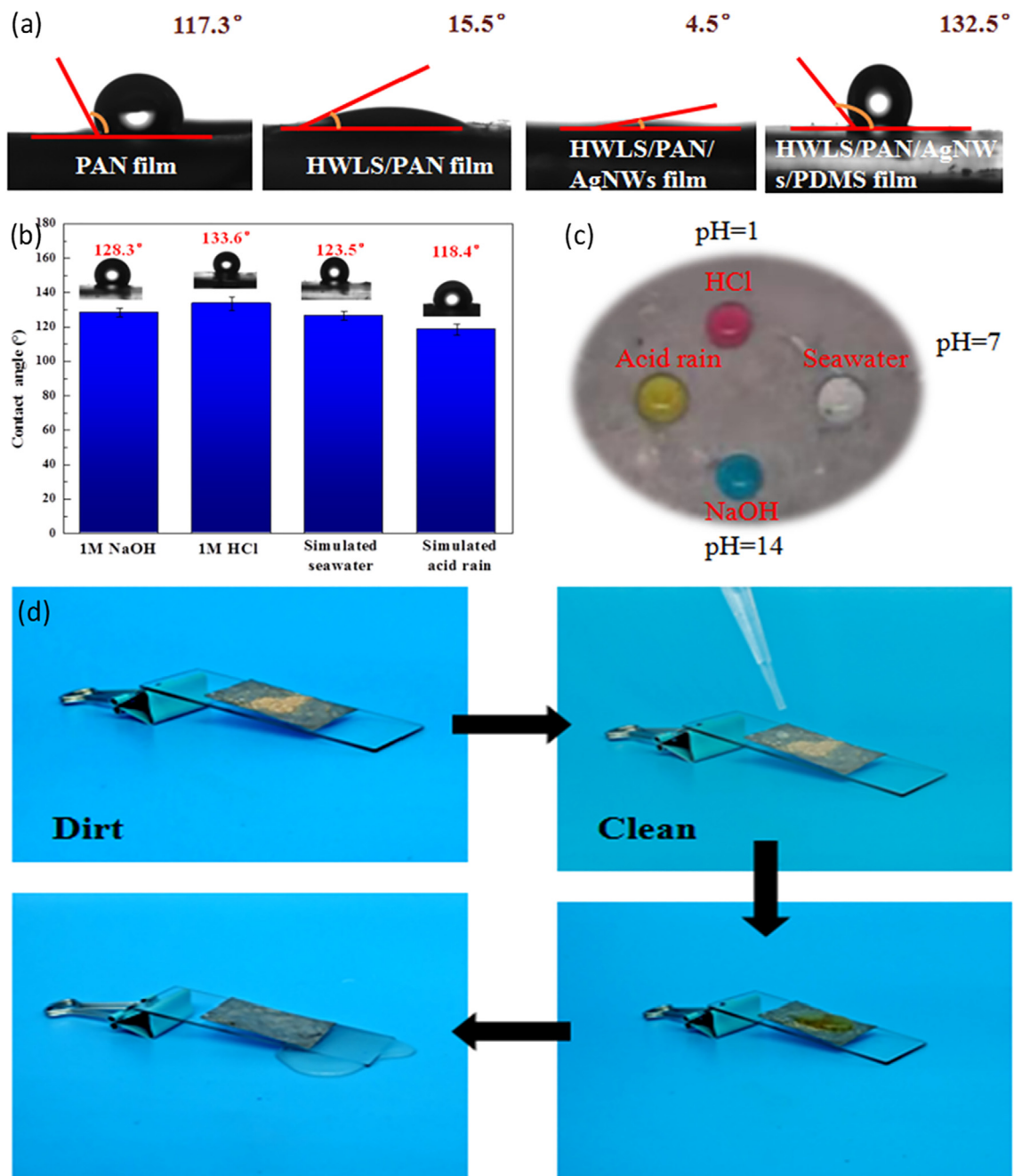


**Fig. 6.** (a) Water contact angle of the PAN, HP, HPA, and HPAP films. (b) Contact angles of an HPAP film with different liquid droplets. Insets are the corresponding photographs. (c) Photographs of different liquid droplets on an HPAP film. (d) Self-cleaning process of coffee powder on a HPAP film.

ing rate, which is important for practical applications. Fig. 7e shows the stable and repeatable current response under applied pressures varying from 10 to 30 kPa, indicating that the contact resistance of the pressure sensor decreased obviously with increasing external pressure.

#### 4. Conclusion

In this study, a multifunctional composite nanofiber film was prepared by the deliberate assembly of hydrolysate of waste leather scraps, polyacrylonitrile, silver nanowires, and polydimethylsiloxane. The nanofiber films, even at a low thickness, demonstrated a high EMI shielding efficiency and could be used as a pressure sensor to monitor human body motions. This remark-

able performance was ascribed to the intimate contacts between the fiber scaffolds and the high electrical conductivity due to the integration of silver nanowires. Results from this study indicate that waste leather scraps can be exploited as a unique precursor for the preparation of value-added functional nanocomposites.

#### Declaration of Competing Interest

The authors declare that they have no known competing financial interests or personal relationships that could have appeared to influence the work reported in this paper.

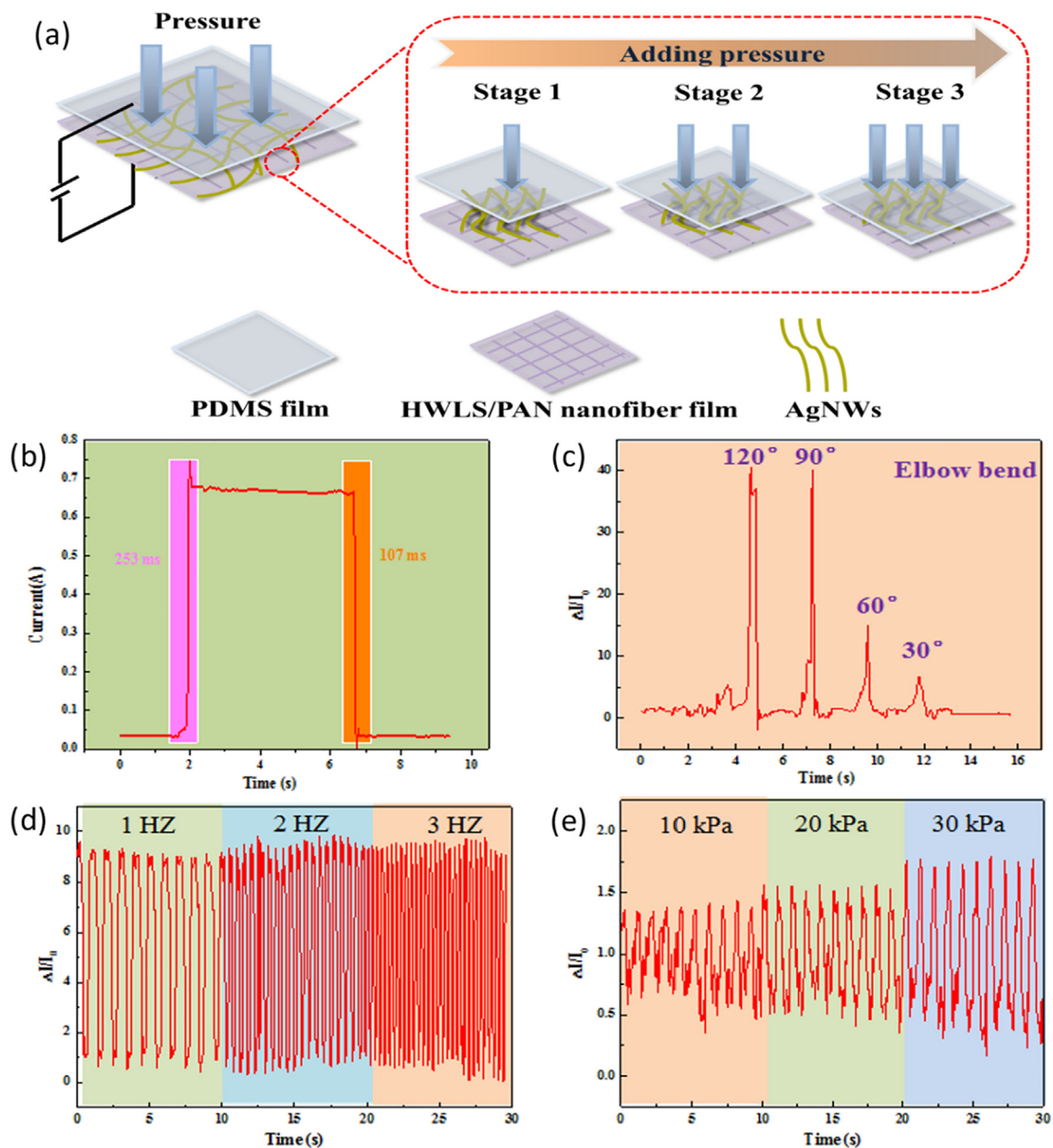


**Fig. 7.** (a) Schematic illustration of the mechanism of the HPAP pressure sensor. (b) Response time and recovery time of the sensor. (c) Original current signals for monitoring elbow bend of a healthy person. (d) Current change of the sensor at different frequencies (1, 2, and 3 Hz). (e) Current change of the sensor at different pressures (10, 20, and 30 kPa).

## Acknowledgments

The work was funded by the National Natural Science Foundation of China (21878182), the Science Foundation for Distinguished Young Scholars of Shaanxi Natural Science Basic Research Program (2020-JC-47), the Shaanxi Province Key Research and Development Plan (2021GY-200), the Shaanxi Provincial “Special Support Plan for High-level Talents”, and the Innovation Capability Support Program of Shaanxi Province (Program No. 2021TD-16).

## Appendix A. Supplementary material

Supplementary data to this article can be found online at <https://doi.org/10.1016/j.jcis.2022.01.043>.

## References

- [1] H. Lv, Z. Yang, H. Xu, L. Wang, R. Wu, An electrical switch-driven flexible electromagnetic absorber, *Adv. Funct. Mater.* 30 (2020) 1907251.
- [2] F. Shahzad, M. Alhabeab, C.B. Hatter, B. Anasori, S.M. Hong, C.M. Koo, Y. Gogotsi, Electromagnetic interference shielding with 2D transition metal carbides MXenes, *Sci.* 353 (2016) 1137–1140.
- [3] V.M. Hong Ng, H. Huang, K. Zhou, P.S. Lee, W. Que, J.Z. Xu, L.B. Kong, Recent progress in layered transition metal carbides and/or nitrides (MXenes) and their composites: synthesis and applications, *J. Mater. Chem. A* 5 (7) (2017) 3039–3068.
- [4] S. Biswas, S.S. Panja, S. Bose, Tailored distribution of nanoparticles in bi-phasic polymeric blends as emerging materials for suppressing electromagnetic radiation: challenges and prospects, *J. Mater. Chem. C* 6 (13) (2018) 3120–3142.
- [5] Z. Zeng, W. Li, N. Wu, S. Zhao, X. Lu, Polymer-Assisted Fabrication of Silver Nanowire Cellular Monoliths: Toward Hydrophobic and Ultraflexible High-Performance Electromagnetic Interference Shielding Materials, *ACS Appl. Mater. Interfaces* 12 (2020) 38584–38592.

- [6] Y. Zheng, Y. Song, T. Gao, S. Yan, H. Hu, F. Cao, Y. Duan, X. Zhang, Lightweight and hydrophobic three-dimensional wood-derived anisotropic magnetic porous carbon for highly efficient electromagnetic interference shielding, *ACS Appl. Mater Interfaces* 12 (2020) 40802–40814.
- [7] E. Hosseini, M. Arjmand, U. Sundararaj, K. Karan, Filler-free conducting polymers as a new class of transparent electromagnetic interference shields, *ACS Appl. Mater Interfaces* 12 (2020) 28596–28606.
- [8] C. Wang, V. Murugadoss, J. Kong, Z. He, X. Mai, Q. Shao, Y. Chen, L. Guo, C. Liu, S. Angaiyah, Overview of carbon nanostructures and nanocomposites for electromagnetic wave shielding, *Carbon* 140 (2018) 696–733.
- [9] M.L. Ma, Y.X. Bi, Z.G. Jiao, J.W. Yue, Z.G. Liao, Y. Wang, Y. Ma, W.B. Huang, Facile fabrication of metal–organic framework derived Fe/Fe<sub>3</sub>O<sub>4</sub>/FeN/N-doped carbon composites coated with PPy for superior microwave absorption, *J. Colloid Interf. Sci.* 608 (2022) 525–535.
- [10] M.L. Ma, Z.G. Liao, X.W. Su, Q.X. Zheng, Y.Y. Liu, Y. Wang, Y. Ma, F. Wang, Magnetic CoNi alloy particles embedded N-doped carbon fibers with polypyrrole for excellent electromagnetic wave absorption, *J. Colloid Interf. Sci.* 608 (2022) 2203–2212.
- [11] S. Lee, I. Jo, S. Kang, B. Jang, J. Moon, J.B. Park, S. Lee, S. Rho, Y. Kim, B.H. Hong, Smart Contact Lenses with Graphene Coating for Electromagnetic Interference Shielding and Dehydration Protection, *ACS Nano* 11 (2017) 5318–5324.
- [12] L.C. Jia, G.Q. Zhang, L. Xu, W.J. Sun, G.J. Zhong, J. Lei, D.X. Yan, Z.M. Li, Robustly Superhydrophobic Conductive Textile for Efficient Electromagnetic Interference Shielding, *ACS Appl. Mater Interfaces* 11 (2019) 1680–1688.
- [13] S. Ghosh, B. Nitin, S. Remanan, Y. Bhattacharjee, A. Ghorai, T. Dey, T.K. Das, N.C. Das, A Multifunctional Smart Textile Derived from Merino Wool/Nylon Polymer Nanocomposites as Next Generation Microwave Absorber and Soft Touch Sensor, *ACS Appl. Mater Interfaces* 12 (2020) 17988–18001.
- [14] J.C. Luo, L.Y. Huo, L. Wang, X.W. Huang, J.Y. Li, Z. Guo, Q. Gao, M.J. Hu, H.G. Xue, J.F. Gao, Superhydrophobic and multi-responsive fabric composite with excellent electro-photo-thermal effect and electromagnetic interference shielding performance, *Chem. Eng. J.* 391 (2020) 123537.
- [15] E. Zussman, X. Chen, W. Ding, L. Calabri, D.A. Dikin, J.P. Quintana, R.S. Ruoff, Mechanical and structural characterization of electrospun PAN-derived carbon nanofibers, *Carbon* 43 (2005) 2175–2185.
- [16] Y.u. Xu, Y. Li, W. Hua, A. Zhang, J. Bao, Light-weight silver plating foam and carbon nanotube hybridized epoxy composite foams with exceptional conductivity and electromagnetic shielding property, *ACS Appl. Mater Interfaces* 8 (36) (2016) 24131–24142.
- [17] S. Lee, J. Park, M.C. Kim, M. Kim, P. Park, I.-J. Yoon, J. Nah, Polyvinylidene Fluoride Core-Shell Nanofiber Membranes with Highly Conductive Shells for Electromagnetic Interference Shielding, *ACS Appl. Mater Interfaces* 13 (21) (2021) 25428–25437.
- [18] N.A. Medellín-Castillo, E.D. Isaacs-Páez, I. Rodríguez-Méndez, R. González-García, G.J. Labrada-Delgado, A. Aragón-Piña, M.E. García-Arreola, Formaldehyde and triphosphosphate crosslinked chitosan hydrogels: Synthesis, characterization and modeling, *Int. J. Biol. Macromol* 183 (2021) 2293–2304.
- [19] M. Hulupi, H. Haryadi, Synthesis and Characterization of Electrospinning PVA Nanofiber-Crosslinked by Glutaraldehyde, *Mater Today-Proc.* 13 (2019) 199–204.
- [20] Y. Liu, S. Shang, S. Mo, P. Wang, H. Wang, Eco-friendly Strategies for the Material and Fabrication of Wearable Sensors, *Int. J. Pr. Eng. Man-Gt.* 8 (4) (2021) 1323–1346.
- [21] J. Liu, D. Yan, W. Pang, Y. Zhang, Design, fabrication and applications of soft network materials, *Mater Today* 49 (2021) 324–350, <https://doi.org/10.1016/j.mattod.2021.05.007>.
- [22] U.P. Claver, G. Zhao, Recent Progress in Flexible Pressure Sensors Based Electronic Skin, *Adv. Eng. Mater* 23 (2021) 2001187.
- [23] M.Q. Jian, K.L. Xia, Q. Wang, Z. Yin, H.M. Wang, C.Y. Wang, H.H. Xie, M.C. Zhang, Y.Y. Zhang, Flexible and Highly Sensitive Pressure Sensors Based on Bionic Hierarchical Structures, *Adv. Funct. Mater* 27 (2017) 1606066.
- [24] Y.X. Li, T.Y. He, L.J. Shi, R.R. Wang, J. Sun, Strain Sensor with Both a Wide Sensing Range and High Sensitivity Based on Braided Graphene Belts, *ACS Appl Mater Interfaces* 12 (2020) 17691–17698.
- [25] Y.A. Chen, Y. Liu, Y.H. Li, H.S. Qi, Highly Sensitive, Flexible, Stable, and Hydrophobic Biofoam Based on Wheat Flour for Multifunctional Sensor and Adjustable EMI Shielding Applications, *ACS Appl. Mater Interfaces* 13 (2021) 30020–30029.
- [26] H. Wu, D. Kong, Z. Ruan, P.-C. Hsu, S. Wang, Z. Yu, T.J. Carney, L. Hu, S. Fan, Y.i. Cui, A transparent electrode based on a metal nanotrout network, *Nat. Nanotechnol* 8 (6) (2013) 421–425.
- [27] A. Miyamoto, S. Lee, N.F. Cooray, S. Lee, M. Mori, N. Matsuhisa, H. Jin, L. Yoda, T. Yokota, A. Itoh, M. Sekino, H. Kawasaki, T. Ebihara, M. Amagai, T. Someya, Inflammation-free, gas-permeable, lightweight, stretchable on-skin electronics with nanomeshes, *Nat. Nanotechnol* 12 (9) (2017) 907–913.
- [28] H.e. Ji, R. Zhao, N. Zhang, C. Jin, X. Lu, C.e. Wang, Lightweight and flexible electrospun polymer nanofiber/metal nanoparticle hybrid membrane for high-performance electromagnetic interference shielding, *Npg Asia Mater* 10 (8) (2018) 749–760.
- [29] J. Zeng, X. Ji, Y. Ma, Z. Zhang, S. Wang, Z. Ren, C. Zhi, J. Yu, 3D graphene fibers grown by thermal chemical vapor deposition, *Adv. Mater* 30 (12) (2018) 1705380, <https://doi.org/10.1002/adma.v30.12.10.1002.adma.201705380>.
- [30] Y. Yao, F. Jiang, C. Yang, K.K. Fu, J. Hayden, C.-F. Lin, H. Xie, M. Jiao, C. Yang, Y. Wang, S. He, F. Xu, E. Hitz, T. Gao, J. Dai, W. Luo, G. Rubloff, C. Wang, L. Hu, Epitaxial Welding of Carbon Nanotube Networks for Aqueous Battery Current Collectors, *ACS Nano* 12 (6) (2018) 5266–5273.
- [31] L. Chen, Y.H. Li, L.N. Chen, N. Li, C.L. Dong, Q. Chen, B.B. Liu, Q. Ai, P.C. Si, J.K. Feng, L. Zhang, J. Suhr, J. Lou, L.J. Ci, A large-area free-standing graphene oxide multilayer membrane with high stability for nanofiltration applications, *Chem. Eng. J.* 345 (2018) 536–544.
- [32] W. Xu, Y. Ding, R. Huang, Z. Zhu, H. Fong, H. Hou, High-performance polyimide nanofibers reinforced polyimide nanocomposite films fabricated by co-electrospinning followed by hot-pressing, *J. Appl. Polym. Sci.* 135 (2018) 46869.
- [33] N. Sun, Z. Wen, F.P. Zhao, Y.Q. Yang, H.Y. Shao, C.J. Zhou, Q.Q. Shen, K. Feng, M. F. Peng, Y.G. Li, X.H. Sun, All flexible electrospun papers based self-charging power system, *Nano Energy* 38 (2017) 210–217.
- [34] Y.T. Wang, H.K. Peng, T.T. Li, B.C. Shiu, H.T. Ren, X.F. Zhang, C.W. Lou, J.H. Lin, MXene-coated conductive composite film with ultrathin, flexible, self-cleaning for high-performance electromagnetic interference shielding, *Chem. Eng. J.* 412 (2021) 128681.
- [35] N. Zhang, R. Zhao, D.Y. He, Y.Y. Ma, J. Qiu, C.X. Jin, C. Wang, Lightweight and flexible Ni-Co alloy nanoparticle-coated electrospun polymer nanofiber hybrid membranes for high-performance electromagnetic interference shielding, *J. Alloy Compd.* 784 (2019) 244–255.
- [36] X. Wang, O. Yue, X. Liu, M. Hou, M. Zheng, A novel bio-inspired multi-functional collagen aggregate based flexible sensor with multi-layer and internal 3D network structure, *Chem. Eng. J.* 392 (2020) 123672, <https://doi.org/10.1016/j.cej.2019.123672>.
- [37] W. Lv, K. Zhao, S. Ma, L. Kong, Z. Dang, J. Chen, Y. Zhang, J. Hu, Process of removing heavy metal ions and solids suspended in micro-scale intensified by hydrocyclone, *J. Clean Prod.* 263 (2020) 121533, <https://doi.org/10.1016/j.jclepro.2020.121533>.
- [38] Z. Joseph, J. Gladstone Christopher, B. Assefa Demessie, A. Tamil Selvi, K.J. Sreeram, J. Raghava Rao, Extraction of elastin from tannery wastes: A cleaner technology for tannery waste management, *J. Clean Prod.* 243 (2020) 118471, <https://doi.org/10.1016/j.jclepro.2019.118471>.
- [39] C. Liu, X. Wang, X. Huang, X. Liao, B.i. Shi, Absorption and Reflection Contributions to the High Performance of Electromagnetic Waves Shielding Materials Fabricated by Compositing Leather Matrix with Metal Nanoparticles, *ACS Appl. Mater. Interfaces* 10 (16) (2018) 14036–14044.
- [40] M. Kim, S. Kim, Y.C. Seong, K.-H. Yang, H. Choi, Multiwalled Carbon Nanotube Buckypaper/Polyacrylonitrile Nanofiber Composite Membranes for Electromagnetic Interference Shielding, *ACS Appl. Nano Mater* 4 (1) (2021) 729–738.
- [41] Y. Liu, F.J. Meng, Y.T. Zhou, S.M. Mugo, Q. Zhang, Graphene Oxide Films Prepared Using Gelatin Nanofibers as Wearable Sensors for Monitoring Cardiovascular Health, *Adv. Mater. Technol.* 4 (2019) 1970059.
- [42] C. Liu, X. Wang, X. Huang, X. Liao, B. Shi, Absorption and reflection contributions to the high performance of electromagnetic waves shielding materials fabricated by compositing leather matrix with metal nanoparticles, *ACS Appl. Mater Interfaces* 10 (2018) 14036–14044.
- [43] C. Liu, X. Ye, X. Wang, X. Liao, X. Huang, B. Shi, Collagen fiber membrane as an absorptive substrate to coat with carbon nanotubes-encapsulated metal nanoparticles for lightweight, wearable, and absorption-dominated shielding membrane, *Ind. Eng. Chem. Res.* 56 (2017) 8553–8562.
- [44] S. Zeng, Z.-X. Huang, H. Jiang, Y. Li, From waste to wealth: A lightweight and flexible leather solid waste/polyvinyl alcohol/silver paper for highly efficient electromagnetic interference shielding, *ACS Appl. Mater Interfaces* 12 (2020) 52038–52049.
- [45] Y. Chen, L. Pang, Y. Li, H. Luo, G. Duan, C. Mei, W. Xu, W. Zhou, K. Liu, S. Jiang, Ultra-thin and highly flexible cellulose nanofiber/silver nanowire conductive paper for effective electromagnetic interference shielding, *Compos. A: Appl. Sci. Manuf.* 135 (2020) 105960, <https://doi.org/10.1016/j.compositesa.2020.105960>.
- [46] T.-W. Lee, S.-E. Lee, Y.G. Jeong, Highly effective electromagnetic interference shielding materials based on silver nanowire/cellulose papers, *ACS Appl. Mater Interfaces* 8 (20) (2016) 13123–13132.
- [47] F. Ren, H. Guo, Z.-Z. Guo, Y.-L. Jin, H.-J. Duan, P.-G. Ren, D.-X. Yan, Highly Bendable and Durable Waterproof Paper for Ultra-High Electromagnetic Interference Shielding, *Polymers-Basel* 11 (9) (2019) 1486, <https://doi.org/10.3390/polym11091486>.
- [48] W.-T. Cao, F.-F. Chen, Y.-J. Zhu, Y.-G. Zhang, Y.-Y. Jiang, M.-G. Ma, F. Chen, Binary Strengthening and Toughening of MXene/Cellulose Nanofiber Composite Paper with Nacre-Inspired Structure and Superior Electromagnetic Interference Shielding Properties, *ACS Nano* 12 (5) (2018) 4583–4593.
- [49] D. Hu, X. Huang, S. Li, P. Jiang, Flexible and durable cellulose/MXene nanocomposite paper for efficient electromagnetic interference shielding, *Compos. Sci. Technol.* 188 (2020) 107995, <https://doi.org/10.1016/j.compscitech.2020.107995>.
- [50] Y. Zhang, L. Wang, J. Zhang, P. Song, Z. Xiao, C. Liang, H. Qiu, J. Kong, J. Gu, Fabrication and investigation on the ultra-thin and flexible Ti<sub>3</sub>C<sub>2</sub>T<sub>x</sub>/co-doped polyaniline electromagnetic interference shielding composite films, *Compos. Sci. Technol.* 183 (2019) 107833, <https://doi.org/10.1016/j.compscitech.2019.107833>.
- [51] Y. Wang, L.-J. Ni, F. Yang, F.-Q. Gu, K. Liang, K. Marcus, Y.-D. Wan, J.-j. Chen, Z.-S. Feng, Facile preparation of a high-quality copper layer on epoxy resin via electroless plating for applications in electromagnetic interference shielding, *J. Mater Chem. C* 5 (48) (2017) 12769–12776.

- [52] J. Yang, X. Liao, G. Wang, J. Chen, F. Guo, W. Tang, W. Wang, Z. Yan, G. Li, Gradient structure design of lightweight and flexible silicone rubber nanocomposite foam for efficient electromagnetic interference shielding, *Chem. Eng. J.* 390 (2020) 124589, <https://doi.org/10.1016/j.cej.2020.124589>.
- [53] H.-B. Zhang, Q. Yan, W.-G. Zheng, Z. He, Z.-Z. Yu, Tough graphene– polymer microcellular foams for electromagnetic interference shielding, *ACS Appl. Mater Interfaces* 3 (3) (2011) 918–924.
- [54] H.M. Zhang, G.C. Zhang, J.T. Li, X. Fan, Z.X. Jing, J.W. Li, X.T. Shi, Lightweight, multifunctional microcellular PMMA/Fe<sub>3</sub>O<sub>4</sub>@MWCNTs nanocomposite foams with efficient electromagnetic interference shielding, *Compos. A-Appl. Sci. Manuf.* 100 (2017) 128–138.
- [55] L.-P. Wu, Y.-Z. Li, B.-J. Wang, Z.-P. Mao, H. Xu, Y. Zhong, L.-P. Zhang, X.-F. Sui, Electroless Ag-plated sponges by tunable deposition onto cellulose-derived templates for ultra-high electromagnetic interference shielding, *Mater Des.* 159 (2018) 47–56.
- [56] H. Zhang, X. Sun, Z. Heng, Y. Chen, H. Zou, M. Liang, Robust and flexible cellulose nanofiber/multiwalled carbon nanotube film for high-performance electromagnetic interference shielding, *Ind. Eng. Chem. Res.* 57 (2018) 17152–17160.
- [57] B. Li, X. Wen, R. Li, Z. Wang, P.G. Clem, H. Fan, Stress-induced phase transformation and optical coupling of silver nanoparticle superlattices into mechanically stable nanowires, *Nat. Commun.* 5 (2014) 4179.